Supplementary Information

Fabrication of strong internal electric field ZnS/Fe_9S_{10} heterostructure for highly efficient sodium ion storage

Chengzhi Zhang,[a,b] Fei Han,*[a,b] Jianmin Ma,[d] Zheng Li,[a,b] Fuquan Zhang,[a,b] Shaohua Xu,[a,b] Hongbo Liu,[a,b] Xuanke Li,[a,b] Jinshui Liu*[a,b] and An-Hui Lu*[c]

[a] *College of Materials Science and Engineering, Hunan University, Changsha 410082, China*

[b] *Hunan Province Key Laboratory for Advanced Carbon Materials and Applied Technology, Hunan University, Changsha, Hunan, 410082, China*

[c] *State Key Laboratory of Fine Chemicals, School of Chemical Engineering, Dalian University of Technology, Dalian 116024, China*

[d] *School of Physics and Electronics, Hunan University, Changsha 410082, China*

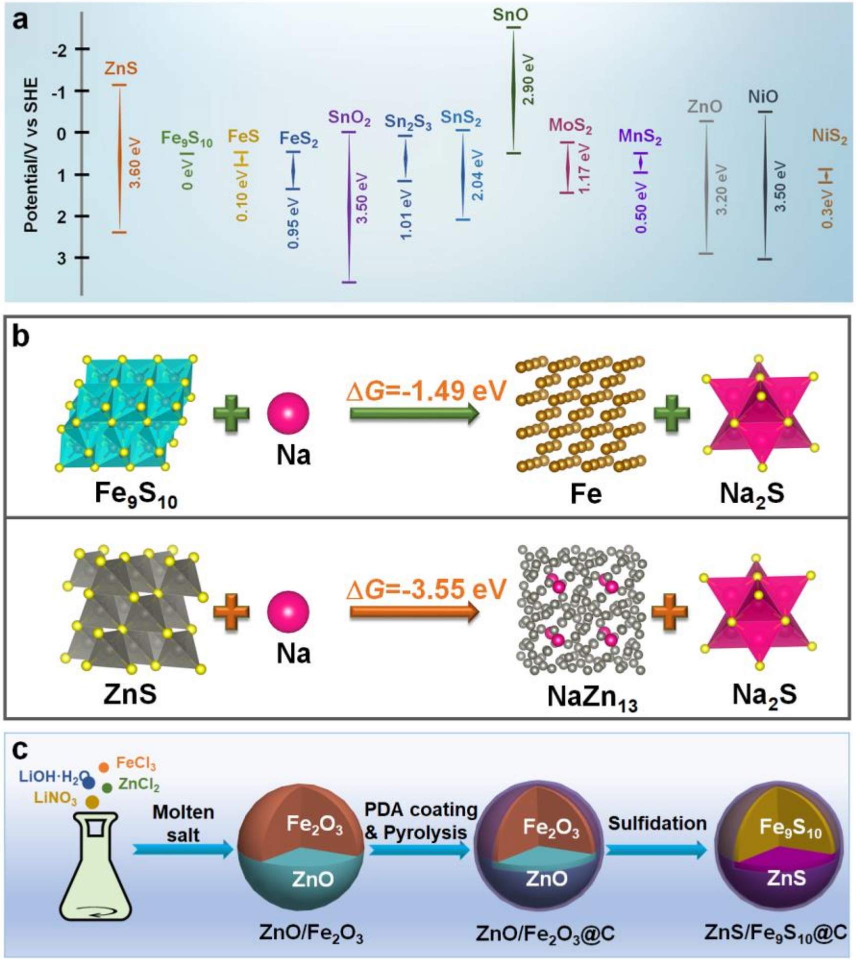

Fig. S1. (a) A summary of the energy bandgaps of common anode materials. (b) The simulated Gibbs free energy changes of Fe_9S_{10} and ZnS active species reacting with sodium. (c) Schematic illustration of the proposed synthetic strategy of $ZnS/Fe_9S_{10}@C$.

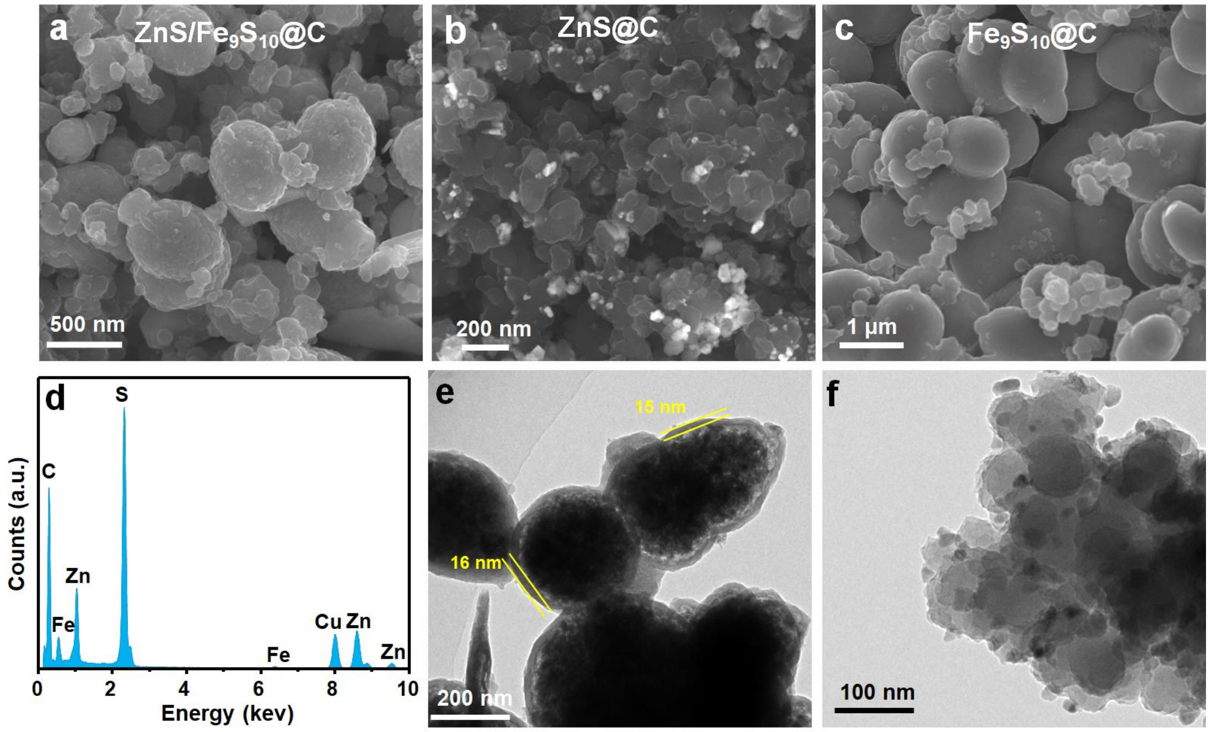

Fig. S2. SEM images of (a) ZnS/Fe_9S_{10}@C, (b) ZnS@C and (c) Fe_9S_{10}@C. (d) EDS spectrum, (e, f) TEM images of ZnS/Fe_9S_{10}@C.

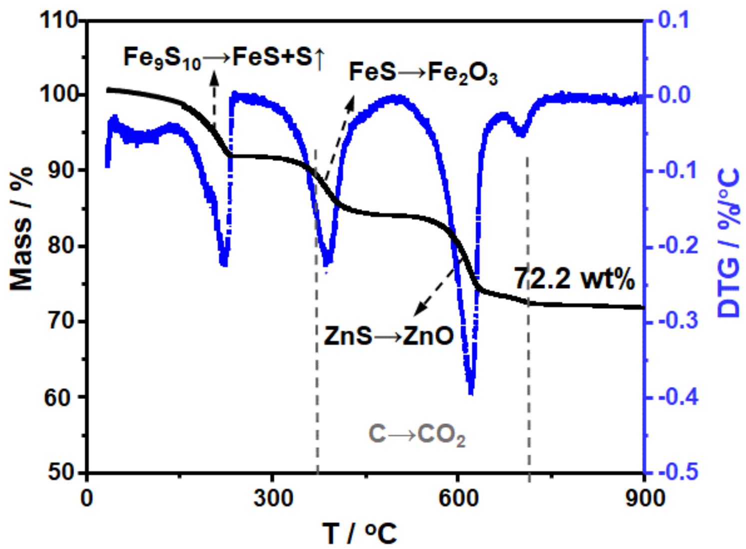

Fig. S3. Thermogravimetric curves of ZnS/Fe_9S_{10}@C thermally treated in air. The chemical processes occurred during the TG test were directly displayed in this figure.

Table S1. A summary of powder electronic conductivity of different samples in this study.

Sample	$ZnS/Fe_9S_{10}@C$	$ZnS@C$	$Fe_9S_{10}@C$	Mixed $ZnS@C-Fe_9S_{10}@C$	$ZnO/Fe_2O_3@C$	ZnO @C	$Fe_2O_3@C$
Powder conductivity ($S\ cm^{-1}$)	6.57×10^{-2}	8.1×10^{-8}	10.1	3.02×10^{-3}	3.51×10^{-5}	8.67×10^{-5}	2.67×10^{-3}

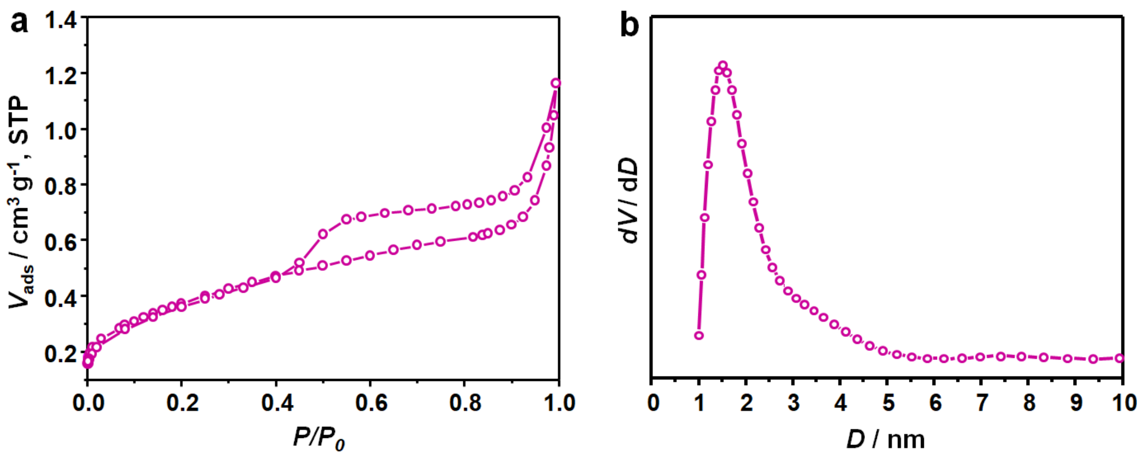

Fig. S4. (a) N_2 sorption isotherm and (b) pore size distribution of $ZnS/Fe_9S_{10}@C$.

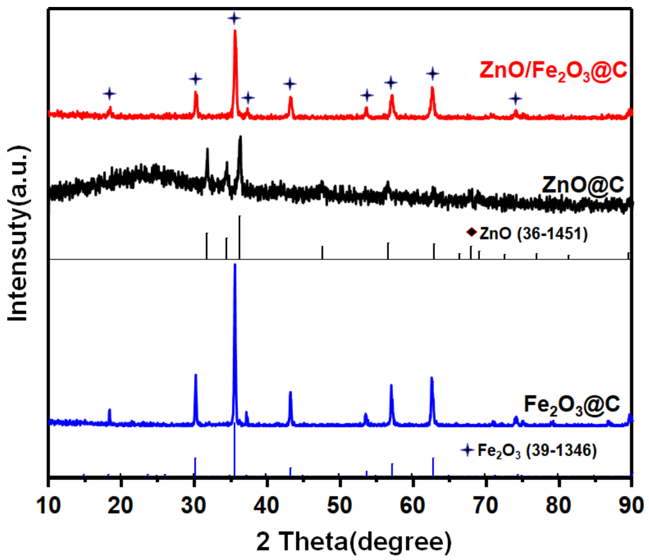

Fig. S5. Wide-angle XRD patterns of $Fe_2O_3@C$, ZnO@C and $ZnO/Fe_2O_3@C$.

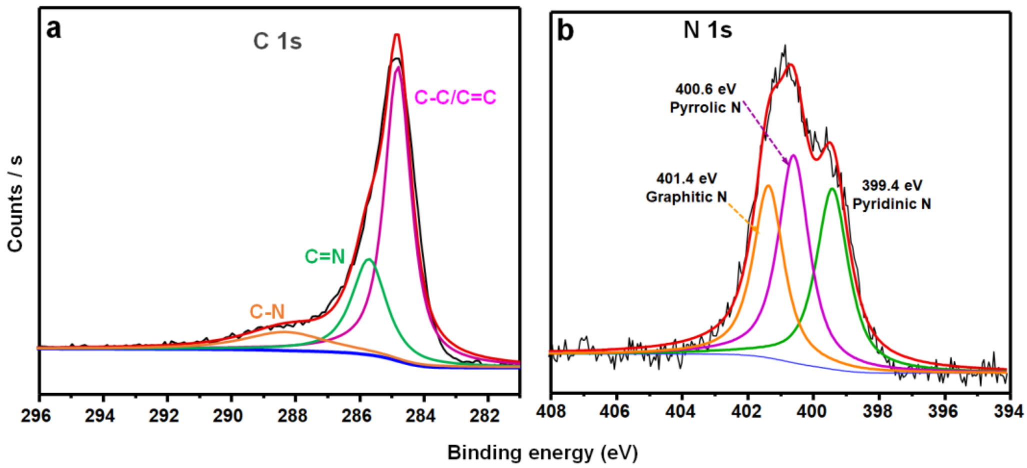

Fig. S6. The high-resolution XPS spectra of C 1s and N 1s of ZnS/Fe_9S_{10}@C.

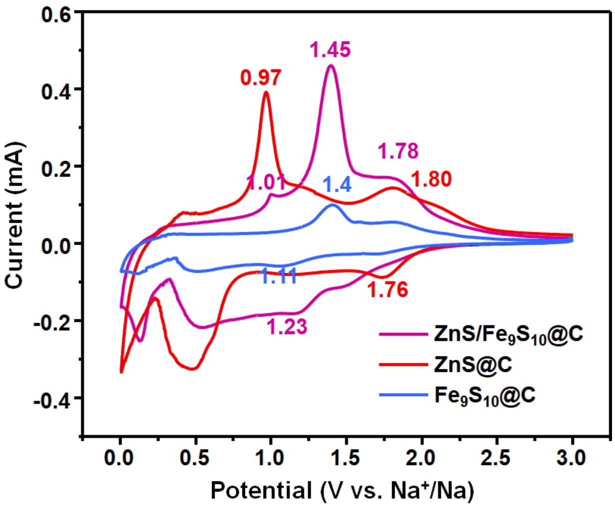

Fig. S7. The typical CV curves of ZnS@C, Fe_9S_{10}@C and ZnS/Fe_9S_{10}@C.

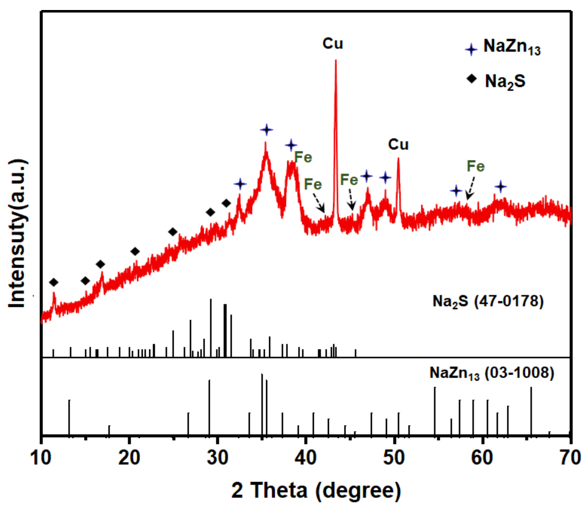

Fig. S8. XRD pattern of the ZnS/Fe_9S_{10}@C electrode under the full sodiation condition.

Table S2. Comparison of the volumetric capacity with recently reported anode materials for Na-ion batteries.

Materials	Volumetric capacity (mAh cm^{-3})	Current density (A g^{-1})	Mass loading (mg cm^{-2})	Density (g cm^{-3})	Ref.
ZnS/Fe_9S_{10}@C	**1030/670/386**	**0.5/10/50**	**1.5**	**1.62**	**This work**
Bi_2Se_3/GNS	379	10	1.13	2.07	1
SnTe/C	430	0.96	2.02	2.01	2
Amorphous MoS_3	1011/635/171	1/10/50	2.8	1.9	3
SnS_2-RGONRP	334/255	1/5	0.78	0.94	4
Nitrogen-Rich Graphene	780/118	0.02/10	1.5	1.5	5

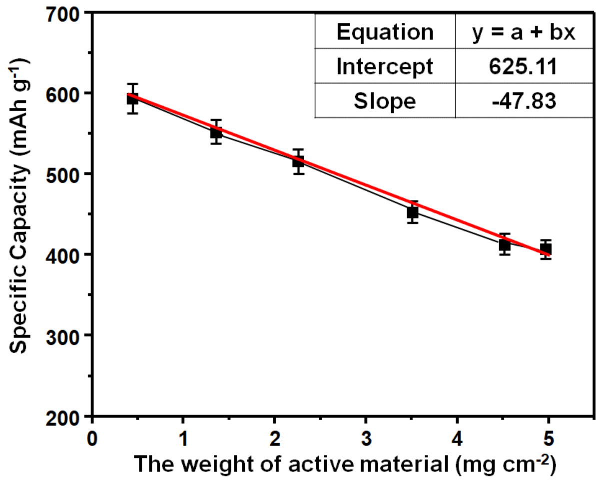

Fig. S9. Half-cell capacities with different loading amounts of ZnS/Fe_9S_{10}@C

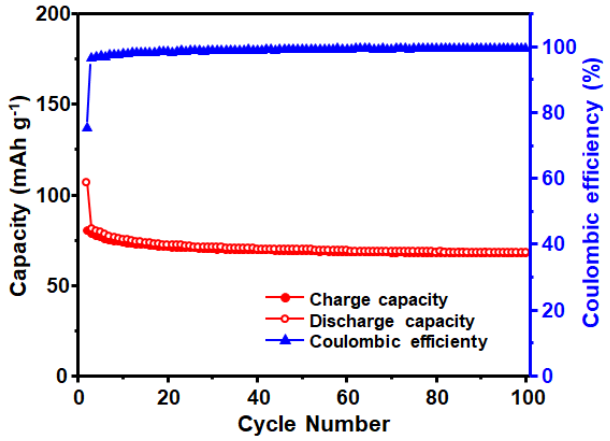

Fig. S10. Cycle performance of pure carbon at a current density of 500 mA g^{-1}. The sample was obtained by etching ZnS/Fe_9S_{10}@C in 1 M HCl solution.

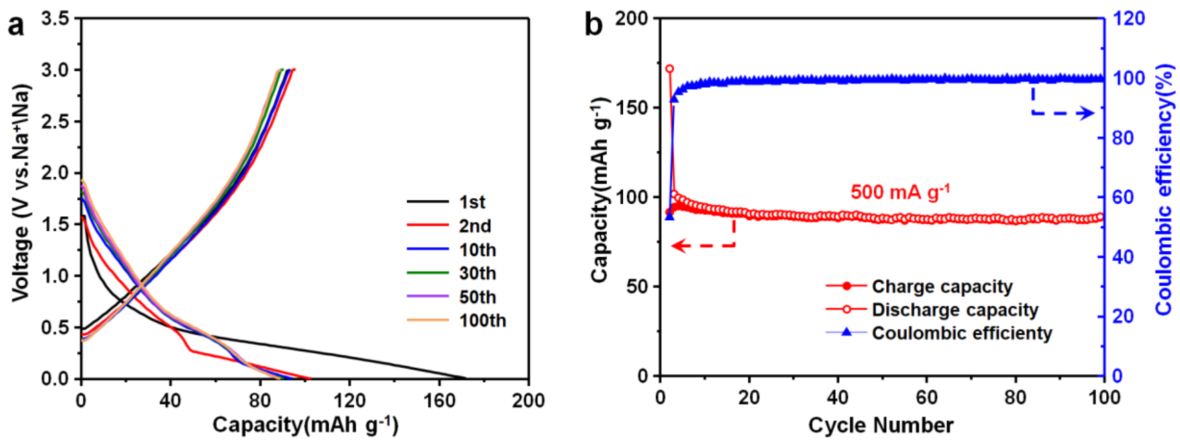

Fig. S11. (a) Galvanostatic discharge/charge profiles and (b) cycle performance of ZnO/Fe_3O_4@C at a current density of 500 mA g^{-1}.

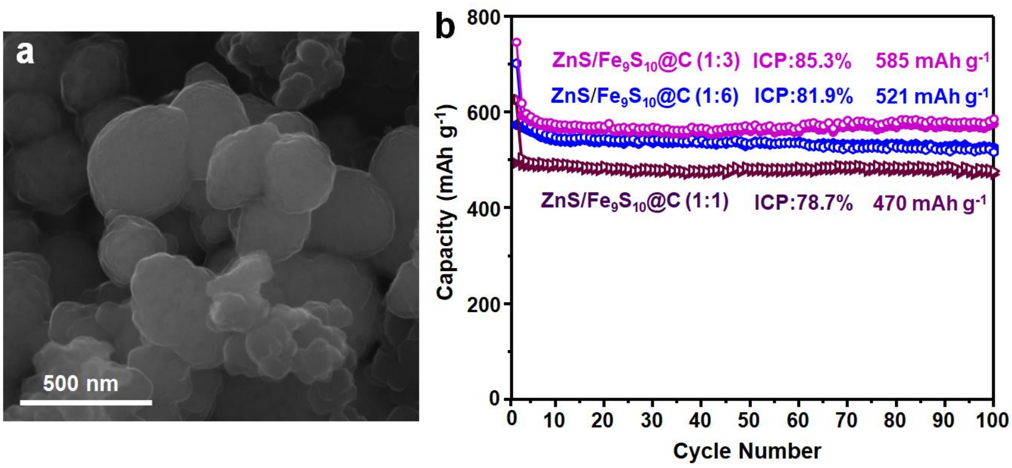

Fig. S12. (a) SEM image of ZnS/Fe_9S_{10}@C with a ZnS/Fe_9S_{10} ratio of 1:1, (b) a comparison of cycle performance of ZnS/Fe_9S_{10}@C with different ZnS/Fe_9S_{10} ratios at 500 mA g^{-1}.

Table S3. Comparison of electrochemical data of $ZnS/Fe_9S_{10}@C$ in this work with previously reported materials zinc sulfide-based, iron sulfide-based and their typical heterogeneous anodes for sodium ion batteries.

Sample	Cut-off voltage (V)	Cycling stability				Rate capability		Ref.
		Current density (A g^{-1})	Initial discapacity (mA h g^{-1})	Cycle number	Capacity retention (mA h g^{-1})	Current density (A g^{-1})	Capacity retention (mA h g^{-1})	
$ZnS/Fe_9S_{10}@C$	**0.005-3**	**1.0**	**688**	**200**	**485**	**50**	**229**	**This work**
Fe_3S_4	0.5-3	0.2	571	100	536	40	233	6
$FeS_2@FeSe_2$ core–shell	0.5-2.9	5.0	–	3850	301	10.0	203	7
Porous FeS nanofibers	0.001-3	0.5	561	150	592	5.0	353	8
$Fe_7S_8@C$ NCs	0.08-3	0.18	–	1000	447	2.7	552	9
$ZnS-Sb_2S_3@C$ Core-Double Shell	0.01-1.8	0.1	–	120	630	0.8	391	10
$FeS_2@C$ yolk–shell	0.1-2	2.0	–	800	330	5.0	403	11
Sb/ZnS@C	0.1-1.8	0.1	–	150	555	1.6	214	12
ZnS/NPC	0.005-3	1	–	1000	456	4.0	182	13
MoS_2/G	0.01-2.7	0.1	–	100	432	50	201	14
$RGO/SnS_2@C$	0.005-3	0.1	691	100	605	3.2	462	15
$Fe_{1-x}S@CNTS$	0.01-2.3	0.5	638	200	449	8	326	16
$MoS_2@C-CMC$	0.01-3	0.08	556	100	286	1	205	17
$Ce-V_5S_8-C$	0.01-3	1	–	500	496	10	344	18

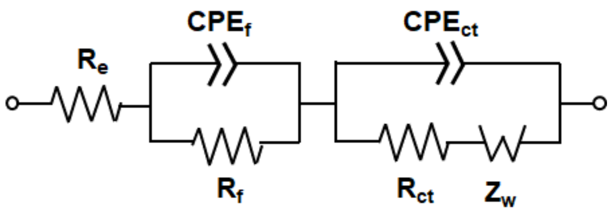

Fig. S13. Equivalent electrical circuit for fitting electrochemical impedance data.

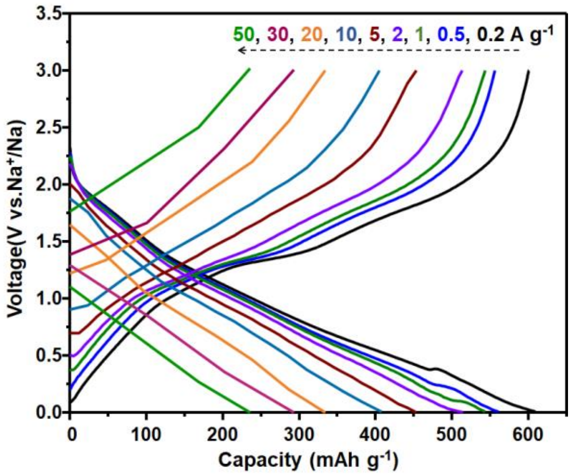

Fig. S14. Typical galvanostatic discharge/charge profiles of ZnS/Fe_9S_{10}@C at different current densities.

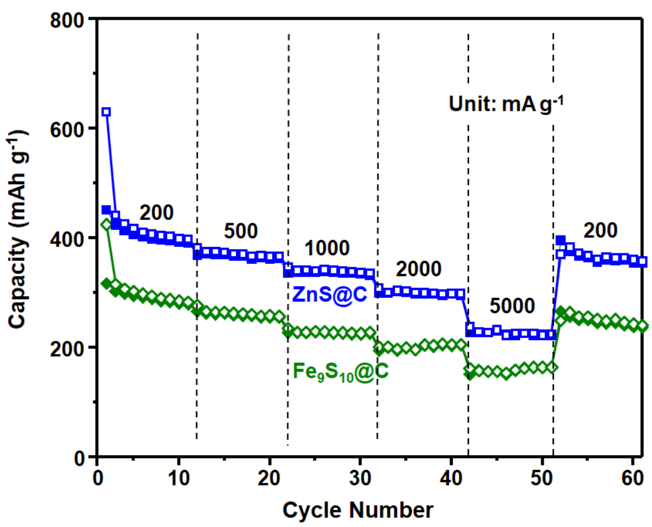

Fig. S15. Rate capability of ZnS@C and Fe_9S_{10}@C with increasing densities from 0.2 to 5.0 A g^{-1}.

Sample	200 mA g^{-1}	500 mA g^{-1}	1000 mA g^{-1}	2000 mA g^{-1}	5000 mA g^{-1}
ZnS@C	412 mAh g^{-1}	371 mAh g^{-1}	340 mAh g^{-1}	300 mAh g^{-1}	228 mAh g^{-1}
Fe_9S_{10}@C	302 mAh g^{-1}	277 mAh g^{-1}	228 mAh g^{-1}	200 mAh g^{-1}	156 mAh g^{-1}

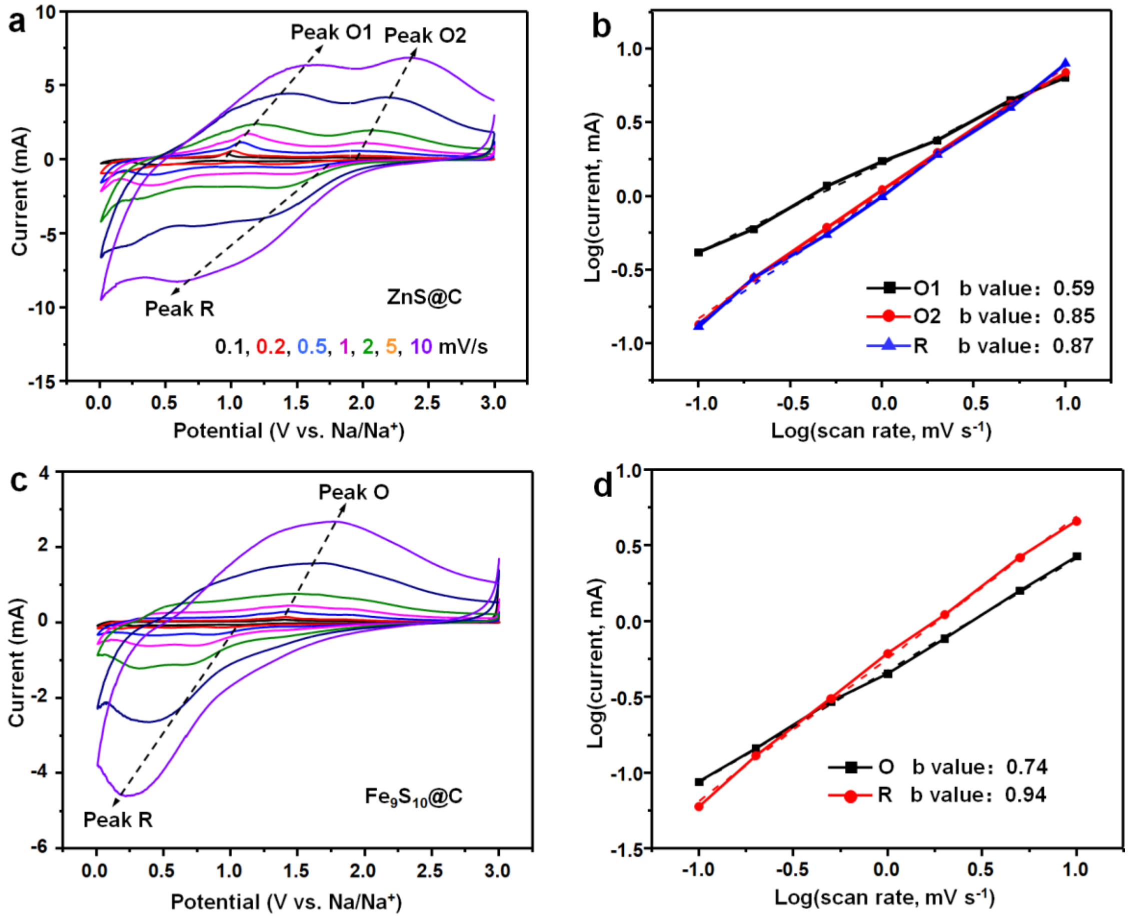

Fig. S16. (a, c) CV curves at different scan rates, and (b, d) current response vs. the scan rate for determining the *b* value of ZnS@C and Fe_9S_{10}@C.

Calculation of the ion diffusion coefficient in samples

The diffusion coefficient of Na^+ can be calculated from the plots in the low frequency region using the following equation:[19]

$$D = \frac{R^2T^2}{2A^2n^4F^4C^2\sigma^2}$$

Where R is the gas constant (8.314 $Jmol^{-1}K^{-1}$), T is the absolute temperature (298.15 K), A is the surface area of the cathode (1.76 cm^2), n is the number of electrons per molecule during oxidization (9.6486×10^4 $Cmol^{-1}$), F is the Faraday constant (96, 486 C mol^{-1}), C is the concentration of Na^+ (8.46×10^{-2} *mol cm*$^{-3}$), and σ is the Warburg factor which obeys the following relationship:

$$Z_{real} = R_e + R_{ct} + \sigma\omega^{-1/2}$$

Where R_e is the resistance between the electrolyte and electrode, and R_{ct} is the charge transfer resistance, ω is angle frequency.

Note: The concentration of Na^+ is calculated according to the complete sodiation reactions of Fe_9S_{10} and ZnS active materials. Considering to the molar ratio of Fe_9S_{10}/ZnS and their respective unit cell volume, the concentration of Na^+ is computed as follows:

$$C=Q_{Na}/\ N_A\ (V_{Fe9S10}+3V_{ZnS}+26.2V_{Na})$$

Where Q_{Na} is total quantity of Na^+, N_A is Avogadro constant 6.02×10^{23}, V_{Fe9S10}, V_{ZnS}, V_{Na} reprensent the unit cell volumes of Fe_9S_{10}, ZnS and Na^+.

Table S4. Kinetic parameters derived from the Nyquist plots of the ZnS@C, Fe_9S_{10}@C and ZnS/Fe_9S_{10}@C after 100 cycles.

	ZnS@C	Fe_9S_{10}@C	ZnS/Fe_9S_{10}@C
Warburg factor (σ)	204	294	72
C (mol cm^{-3})	7.32×10^{-2}	8.89×10^{-2}	8.46×10^{-2}
Diffusion coefficient (*D*) (cm^2 s^{-1})	5.65×10^{-15}	1.87×10^{-15}	3.38×10^{-14}

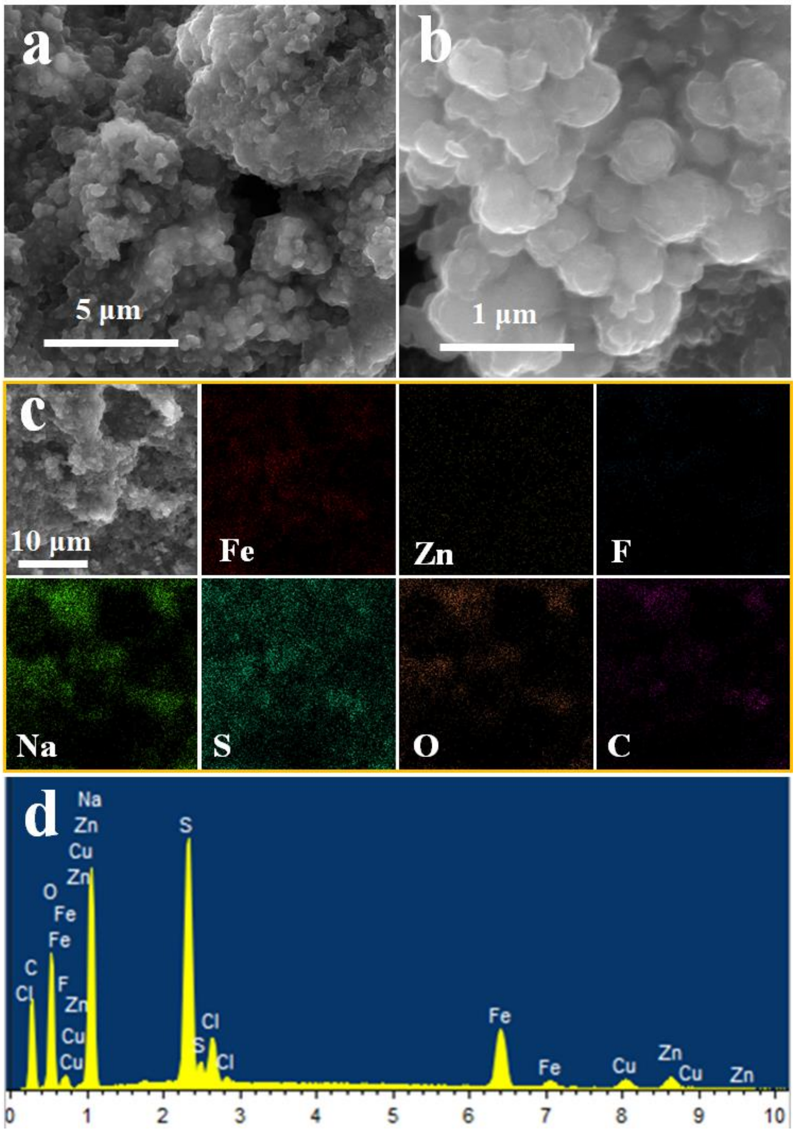

Fig. S17. (a,b) SEM images of $ZnS/Fe_9S_{10}@C$ after 50 cycles under the full discharge condition, and (c) its corresponding elemental mappings and (d) EDS spectrum.

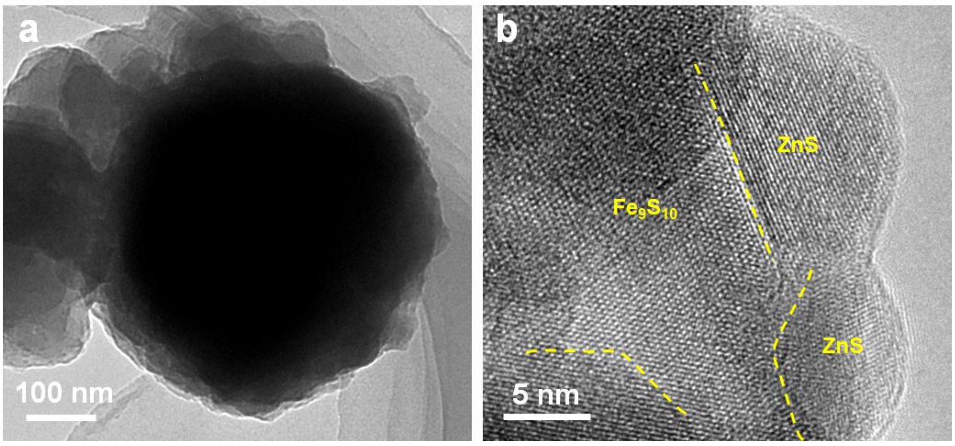

Fig. S18. (a,b) TEM images of $ZnS/Fe_9S_{10}@C$ after 50 cycles under the full charge condition.

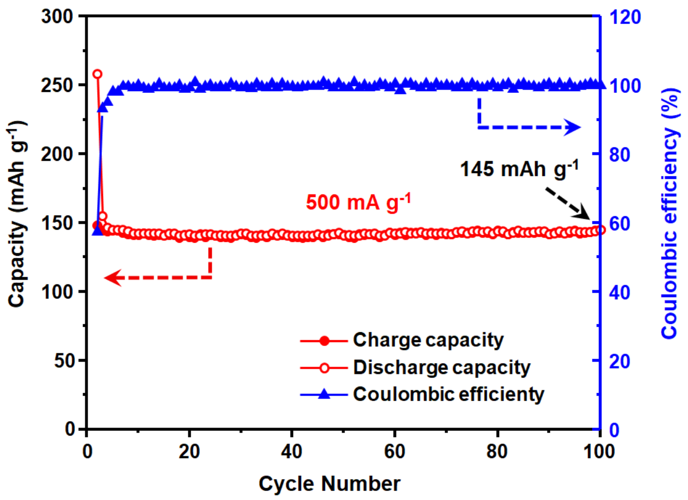

Fig. S19. Cycle performance of $ZnO/SnO_2@C$ at a current density of 500 mA g^{-1}.

References

1 D. Li, J. Zhou, X. Chen and H. Song, *ACS Appl. Mater. Interfaces,* 2018, **10**, 30379-30387.

2 A. R. Park and C. M. Park, *ACS Nano*, 2017, **11**, 6074-6084.

3 H. Ye, W. Lu, S. Deng, X. Zeng and J. Lu, *Adv. Energy Mater.*, 2016**, 7**, 1601602.

4 Y. Liu, Y. Yang, X. Wang, Y. Dong, Y. Tang, Z. Yu, Z. Zhao and J. Qiu, *ACS Appl. Mater. Interfaces*, 2017**, 9**, 15484-15491.

5 Z. Liu, L. H. Zhang, L. Z. Sheng, Q. H. Zhou, T. Wei, J. Feng and Z. J. Fan, *Adv. Energy Mater.*, 2018**,** 8, 1802042.

6 Q. Li, Q. Wei, W. Zuo, L. Huang, W. Luo, Q. An, V. O. Pelenovich, L. Q. Mai and Q. Zhang, *Chem. Sci.*, 2017, **8**, 160-164.

7 W. Zhao, C. Guo and C. Li, *J. Mater. Chem. A*, 2017, **5**, 19195-19202.

8 J. Cho, J. Park and Y. Kang, *Nano Res.*, 2017, **10**, 897-907.

9 M. Choi, J. Kim, J. Yoo, S. Yim, J. Jeon and Y. Jung, *Small*, 2018, **14**, 1702816.

10 S. Dong, C. Li, X. Ge, Z. Li, X. Miao and L. Yin, *ACS Nano*, 2017, **11**, 6474-6482.

11 Z. Liu, T. Lu, T. Song, X. Yu, X. Lou and U. Paik, *Energy Environ. Sci.*, 2017, **10**, 1576-1580.

12 S. Dong, C. Li, Z. Li, L. Zhang and L. Yin, *Small*, 2018, **14**, 1704517.

13 J. Li, D. Yan, X. Zhang, S. Hou, T. Lu, Y. Yao and L. Pan, *J. Mater. Chem. A*, 2017, **5**, 20428-20438.

14 D. Sun, D. Ye, P. Liu, Y. Tang, J. Guo, L. Wang and H. Wang, *Adv. Energy Mater.*, 2018, **8**, 1702383.

15 B. Luo, Y. Hu, X. Zhu, T. Qiu, L. Zhi, M. Xiao, H. Zhang, M. Zou, A. Cao and L. Wang,

J. Mater. Chem. A, 2018, **6**, 1462-1472.

16 Y. Xiao, J. Hwang, I. Belharouak and Y. Sun, *ACS Energy Lett.*, 2017, **2**, 364-372.

17 X. Xie, T. Makaryan, M. Zhao, K. L. Van Aken, Y. Gogotsi and G. Wang, *Adv. Energy Mater.*, 2016, **6**, 1502161.

18 C. Yang, X. Ou, X. Xiong, F. Zheng, R. Hu, Y. Chen, M. Liu and K. V. Huang, *Energy Environ. Sci.*, 2017, **10**, 107-113.

19 X. Du, W. He, X. Zhang, Y. Yue, H. Liu, X. Zhang, D. Min, X. Ge and Y. Du, *J. Mater. Chem.*, 2012, **22**, 5960-5969.